Inorg. Chem. **2008**, *47*, 9344−9350

$BaIrIn_4$ and $Ba_2Ir_4In_{13}$: Two In-Rich Polar Intermetallic Structures with Different Augmented Prismatic Environments about the Cations

Andriy M. Palasyuk and John D. Corbett*

Ames Laboratory-DOE and Department of Chemistry, Iowa State University, Ames, Iowa 50011

Received April 4, 2008

The title phases were synthesized via high-temperature reactions of the elements in welded Ta tubes and characterized by single-crystal X-ray diffraction methods and band calculations. $BaIrIn_4$ adopts the $LaCoAl_4$-type structure: *Pmma*, $Z = 2$, $a = 8.642(2)$, $b = 4.396(1)$, and $c = 7.906(2)$ Å. $Ba_2Ir_4In_{13}$ exhibits a new structure type: $Cmc2_1$, $Z = 4$, $a = 4.4856(9)$, $b = 29.052(6)$, and $c = 13.687(3)$ Å. $BaIrIn_4$ is constructed from a single basic unit, a Ba-centered pentagonal prism of indium on which two adjacent and the opposed rectangular faces are capped by In and Ir, respectively. The three capping atoms are coplanar with Ba and represent the only augmentation of the pentagonal prism. The relatively large proportions of Ba:Ir, In, and of In:Ir lead to the condensation of homoatomic pentagonal prisms into zigzag chains through the sharing of the two uncapped faces. The cation proportion is much lower in $Ba_2Ir_4In_{13}$, and Ba atoms are surrounded by a more anionic Ir/In network without any condensation between prisms. This and the greater Ir proportion lead to a network of formal augmented pentagonal $Ba@Ir_5In_{15}$ and hexagonal $Ba@Ir_7In_{15}$ prisms with overall 5−10−5 and 6−10−6 arrangements of parallel planar rings, respectively, although most Ir is not well bound to the prisms. The latter prism, with alternating Ir/In atoms in the basal faces, is novel for Ae−T−In phases (Ae = alkaline-earth metal, T = Co, Rh, Ir). Band structure calculation results (linear-muffin-tin-orbital method in the atomic sphere approximation) emphasize the greater overlap populations (∼strengths) of the Ir−In bonds and confirm expectations that both compounds are metallic. The Ir 5d bands are narrower and lie higher in energy than those for Au in analogous phases.

Introduction

Polar intermetallics containing triel (p) elements (Tr = Al−Tl) and electropositive alkali (A) or alkaline-earth metals (Ae, Ca−Ba) deviate from Zintl concepts and classical valence viewpoints. Even the binary compounds show evidently novel bonding features that do not fit into the common models.[1−3] For example, K_8In_{11}[4] and $K_{10}Tl_7$[5] exhibit excess cation and electron counts relative to applicable valence rules, whereas $Na_4K_6Tl_{13}$[6] is electron-deficient with respect to an electronically balanced compound because of exceptionally effective packing. The complexity of the structures, especially the degrees of condensation among the more electronegative elements, increases with higher-charged cations or lower proportions of the active metal component, such as in $SrIn_4$[7] and $K_{39}In_{80}$.[8]

Moreover, the addition of the electron-poorer late transition (d) elements such as Ir, Pt, and Au to these binary systems further removes the products from classical closed-shell formulations and into the less well understood area of polar intermetallic networks. Typically, the alkali or alkaline -earth metals are encapsulated in three-dimensional network structures. The nominal polyanionic environments about the cations are often regular pentagonal or hexagonal prisms with diverse augmentations about their waists. The heavier and more electronegative d^{10} or $d^{10}s^1$ transition metals (T) increase the polarity in the networks, bringing additional stabilization (Madelung or bond energies). Thus, stronger

* Author to whom correspondence should be addressed. E-mail: jdc@ameslab.gov.

(1) (a) Nesper, R. *Angew. Chem., Int. Ed. Engl.* **1991**, *30*, 789. (b) Belin, C. H. E.; Tillard-Carbonnel, M. *Prog. Solid State Chem.* **1993**, *22*, 5.
(2) (a) Corbett, J. D. In *Chemistry, Structure and Bonding of Zintl Phases and Ions*; Kauzlarich, S. M., Ed.; VCH Publishers: New York, 1996; Chapter 4. (b) Corbett, J. D. *Angew. Chem., Int. Ed.* **2000**, *39*, 670.
(3) Miller, G. J.; Lee, C.-S.; Choe, W. In *Inorganic Chemistry Highlights*; Meyer, G., Naumann, D., Wesemann, L., Eds.; Wiley-VCH Verlag-Gmbh: Weinheim, Germany, 2002; Chapter 2.
(4) Sevov, S. C.; Corbett, J. D. *Inorg. Chem.* **1991**, *30*, 4877.
(5) Kaskel, S.; Corbett, J. D. *Inorg. Chem.* **2000**, *39*, 3086.
(6) Dong, J.-C.; Corbett, J. D. *J. Am. Chem. Soc.* **1995**, *117*, 6447.
(7) Seo, D.-K.; Corbett, J. D. *J. Am. Chem. Soc.* **2000**, *122*, 9621.
(8) Li, B.; Corbett, J. D. *Inorg. Chem.* **2003**, *42*, 8768.

10.1021/ic8006124 CCC: $40.75 © 2008 American Chemical Society
Published on Web 09/17/2008

heteroatomic T−Tr bonds replace weaker homoatomic Tr−Tr bonds, especially for the sixth period T, and this also increases the flexibility and variety of condensation modes of polyanionic networks. Additionally, these late 5d metals exhibit strong relativistic effects,[9] which serve, for example, to shorten network bonds and lower cell volumes upon isomorphous substitution of T for In. Clear notice of all of these effects was first achieved for the Tr-richer compounds Ba_2AuTl_7,[10] $BaAuTr_3$ ($BaAl_4$ type, Tr = In, Tl),[11] $BaAu_xTr_{2-x}$,[12] and $AeAu_2In_2$ (Ae = Sr, Ba).[13] In this work, we turn to Ir for structural and electronic similarities and differences, some of which presumably occur because of a lower number of valence electrons and a smaller relativistic effect.

Herein, we report on two new In-rich Ba−Ir−In compounds with nominal augmented pentagonal and hexagonal environments around the cations. One of them is a member of a well-known family of 1:1:4 phases, which adopt two different structure types, $YNiAl_4$[14] (*Cmcm*) and $LaCoAl_4$[15] (*Pmma*), supposedly because of different electron concentrations (VEC). This applies for dipositive cations and group 10 (11) T atoms in $CaTIn_4$ (T = Ni, Pd),[15,16] $SrTIn_4$ (T = Ni, Pd, Pt),[17] $EuTIn_4$ (T = Ni, Pd, Cu),[15,18−21] and $YbTIn_4$ (T = Ni, Pd),[18,20] which all crystallize in the $YNiAl_4$ type, whereas the title $BaIrIn_4$ together with $CaTIn_4$ (T = Rh, Ir),[16] $SrIrIn_4$,[22] and $YbRhIn_4$[18] with group 9 T elements and a lower VEC all adopt the $LaCoAl_4$-type structure. The new composition and structure for $Ba_2Ir_4In_{13}$ is the second Ae−T−In compound (the first is $SrRh_2In_8$[22]) with a nominal 20-vertex $Ae@T_5In_{15}$ polyhedron as one of its two basic building units.

Experimental Section

Syntheses. The high-purity reagents were dendritic Ba (99.9%, Alfa-Aesar), Ir sheet (99.997%, Ames Laboratory), and In teardrops (99.99%, Alfa-Aesar). These were handled in N_2-filled gloveboxes in which the moisture levels were maintained below 0.1 ppm (vol). The surfaces of barium and indium were cut clean with a scalpel just before use. The reactions were carried out in welded Ta containers that were in turn sealed within evacuated fused silica jackets and heated in resistance furnaces.[23]

All reactions were run at 950 °C for 120 h, then quenched in water, annealed at 500 °C for 20 d, and quenched again. Well-formed single crystals of $BaIrIn_4$ and $Ba_2Ir_4In_{13}$ were first obtained in at least 95% (no visible impurity lines) and about 90% yields (with extra lines of an unidentified phase) from reactions with Ba/Ir/In = 1:1:4 and 1:2:7, respectively. A substantially pure single phase of $Ba_2Au_4In_{13}$ was obtained in about 95% (or higher) yield after a reaction of the refined composition. Both compounds have a silvery metallic luster and are not very air-sensitive at room temperature, remaining 5−7 days without visible change. Judgements about phase purities in these cases were made on the basis of comparisons of the Guinier powder patterns with those calculated from the refined structures (as illustrated in the Supporting Information). The absence of unidentified lines in patterns of samples loaded with the refined compositions and thus judged to be >95% pure is powerful evidence that the refined compositions are correct (in the absence of any glassy phase, of course).

Powder X-Ray Diffraction. Powder diffraction data were collected with the aid of a Huber 670 Guinier powder camera equipped with an area detector and Cu Kα radiation ($\lambda = 1.540598$ Å). Powdered samples were homogeneously dispersed in a glovebox between two Mylar sheets with the aid of a little vacuum grease. These were in turn held between split Al rings that provided airtight seals. Unit cell parameters were refined with the WinXPow program.[24]

Structure Determinations. Single crystals were selected from the products in a glovebox and, as an early precaution, sealed into capillaries. Single-crystal diffraction data for both title compounds were collected at 293(2) K with the aid of Mo Kα radiation and a Bruker SMART APEX CCD diffractometer, each in the form of three sets of 606 frames with 0.3° scans in ω and exposure times of 10 s per frame. The 2θ range extended from ∼3° to ∼57°. The reflection intensities were integrated with the SAINT subprogram in the SMART software package.[25] The space groups suggested by the XPREP program in the SHELXTL 6.1 software package[26] were $Pmc2_1$ (No. 26), *Pmma* (No. 51), and *Pma*2 (No. 28) for $BaIrIn_4$ and $Cmc2_1$ (No. 36), *Cmcm* (No. 63), and *Ama*2 (No. 40) for $Ba_2Ir_4In_{13}$. The intensity statistics for the data set from the former gave very clear indications of centricity ($|E^2 - 1| = 0.864$), whereas an obvious hint of a noncentrosymmetric space group occurred for the 2:4:13 phase ($|E^2 - 1| = 0.676$). The refinements proceeded successfully in centrosymmetric *Pmma* and noncentrosymmetric $Cmc2_1$ groups. Empirical absorption corrections for each compound were made with the aid of the SADABS program.[27] Each structure was solved by direct methods with the aid of SHELXTL 6.1 and refined by full-matrix least-squares on F_o^2, ultimately with anisotropic thermal parameters and a secondary extinction parameter. The refinements converged at R1 = 0.023 and wR2 = 0.058 and at R1 = 0.038 and wR2 = 0.089 ($I > 2\sigma(I)$) for $BaIrIn_4$ and $Ba_2Ir_4In_{13}$, respectively. All positions appeared to be fully occupied by single atom types. The largest residual peak and hole in the ΔF map were 1.70 and −2.88 $e\cdot$Å^{-3} and 2.14 and −2.75 $e\cdot$Å^{-3}, respectively. Some crystallographic data for each phase are summarized in Table 1, and the atom positions are listed in Table 2. More detailed crystallographic and refinement information as well as anisotropic displacement parameters are available in the Supporting Information (CIF).

(9) (a) Pyykö, P. *Chem. Rev.* **1998**, *88*, 63. (b) Pyykö, P. *Angew. Chem., Int. Ed.* **2002**, *41*, 3573.
(10) Liu, S.; Corbett, J. D. *Inorg. Chem.* **2004**, *43*, 2471.
(11) Liu, S.; Corbett, J. D. *Inorg. Chem.* **2004**, *43*, 4988.
(12) Dai, J.-C.; Corbett, J. D. *Inorg. Chem.* **2006**, *45*, 2104.
(13) Dai, J.-C.; Corbett, J. D. *Inorg. Chem.* **2007**, *46*, 4592.
(14) Rykhal', R. M.; Zarechnyuk, O. S.; Yarmolyuk, Ya. P. *Sov. Phys. Crystallogr.* **1972**, *17*, 453.
(15) Sysa, L. V.; Kalychak, Y. M. *Crystallogr. Rep.* **1993**, *8*, 278.
(16) Hoffmann, R.-D.; Pöttgen, R. *Chem.—Eur. J.* **2000**, *6*, 600.
(17) Muts, I.; Zaremba, V. I.; Baran, V. V.; Pöttgen, R. *Z. Naturforsch. B* **2007**, *62*, 1407.
(18) Hoffmann, R.-D.; Pöttgen, R.; Zaremba, V. I.; Kalychak, Ya. M. *Z. Naturforsch.* **2000**, *55b*, 834.
(19) Sysa, L. V.; Kalychak, Y. M. *Crystallogr. Rep.* **1993**, *8*, 278.
(20) Kalychak, Ya. M.; Baranyak, V. M.; Zaremba, V. I.; Zavalii, P. Yu.; Dmytrakh, O. V.; Bruskov, V. A. *Sov. Phys. Crystallogr.* **1988**, *33*, 302.
(21) Pöttgen, R.; Muellmann, R.; Mosel, B. D.; Eckert, H. *J. Matter. Chem.* **1996**, *6*, 801.
(22) Muts, I.; Zaremba, V. I.; Pöttgen, R. *Z. Anorg. Allg. Chem.* **2007**, *633*, 2234.
(23) Corbett, J. D. *Inorg. Synth.* **1983**, *22*, 15.
(24) *STOE WinXPow 2.10*; STOE & Cie GmbH: Hilpertstr. Darmstadt, Germany, 2004.
(25) *SMART*; Bruker AXS, Inc.: Madison, WI, 1996.
(26) *SHELXTL*, version 5.1; Bruker AXS, Inc.: Madison, WI, 1998.
(27) Blessing, R. H. *Acta Crystallogr.* **1995**, *A51*, 33.

Table 1. Some Crystal and Refinement Data for $BaIrIn_4$ and $Ba_2Ir_4In_{13}$

compounds	$BaIrIn_4$	$Ba_2Ir_4In_{13}$
fw	788.8	2536.1
space group, Z	*Pmma* (No.51), 2	$Cmc2_1$ (No.36), 4
unit cell (Å), a	8.642(2)	4.4856(9)
b	4.396(1)	29.052(6)
c	7.906(2)	13.687(3)
V(Å^3)	300.3(1)	1783.6(6)
d_{calcd} (Mg/m^3)	8.72	9.44
μ, mm^{-1} (Mo Kα)	43.5	50.4
reflns collected/R_{int}	1797/0.0305	5556/0.0379
ind. data/restraints/params	422/0/24	2122/1/116
goodness of fit on F^2	1.149	1.065
$R1/wR2$ [$I > 2\sigma(I)$]	0.0234/0.0577	0.0381/0.0886
$R1/wR2$ (all data)	0.0240/0.0580	0.0400/0.0896
largest diff. peak and hole (e•Å^{-3})	1.70, −2.88	2.14, −2.75

Table 2. Atomic Coordinates and Isotropic-Equivalent Displacement Parameters (Å$^2 \times 10^3$) for $BaIrIn_4$ and $Ba_2Ir_4In_{13}$

atom	Wyckoff position	symmetry	x	y	z	U(eq)
			$BaIrIn_4$			
Ba	2*e*	*mm*2	1/4	0	0.60801(9)	11(1)
Ir	2*e*	*mm*2	1/4	0	0.18371(6)	8(1)
In1	4*j*	.*m*.	0.06853(9)	1/2	0.29910(8)	11(1)
In2	2*f*	*mm*2	1/4	1/2	0.9453(1)	10(1)
In3	2*a*	.2/*m*.	0	0	0	13(1)
			$Ba_2Ir_4In_{13}$			
Ba1	4*a*	*m*..	0	0.45988(6)	0.8941(2)	8(1)
Ba2	4*a*	*m*..	0	0.25175(6)	0.5719(2)	12(1)
Ir1	4*a*	*m*..	0	0.41155(4)	0.5832(1)	5(1)
Ir2	4*a*	*m*..	0	0.30885(3)	0.8945(1)	6(1)
Ir3	4*a*	*m*..	0	0.41805(4)	0.20267(9)	5(1)
Ir4	4*a*	*m*..	0	0.31532(4)	0.26452(9)	8(1)
In1	4*a*	*m*..	0	0.92846(7)	0.7146(2)	8(1)
In2	4*a*	*m*..	0	0.35302(7)	0.7294(2)	10(1)
In3	4*a*	*m*..	0	0.49724(8)	0.6406(2)	9(1)
In4	4*a*	*m*..	0	0.96313(8)	0.2868(2)	9(1)
In5	4*a*	*m*..	0	0.38522(7)	0.3948(2)	10(1)
In6	4*a*	*m*..	0	0.86288(8)	0.9076(2)	9(1)
In7	4*a*	*m*..	0	0.93200(7)	0.0713(2)	8(1)
In8	4*a*	*m*..	0	0.95500(8)	0.4971(2)	8(1)
In9	4*a*	*m*..	0	0.86031(8)	0.2282(2)	9(1)
In10	4*a*	*m*..	0	0.84925(7)	0.5573(2)	10(1)
In11	4*a*	*m*..	0	0.77472(7)	0.7886(2)	10(1)
In12	4*a*	*m*..	0	0.34445(7)	0.0716(2)	8(1)
In13	4*a*	*m*..	0	0.21514(7)	0.8767(2)	9(1)

Electronic Structure Calculations. In order to understand the chemical bonding better, tight-binding electronic structure calculations were performed for both structures by the linear-muffin-tin-orbital (LMTO) method in the atomic sphere approximation (ASA).[28] The radii of the Wigner-Seitz (WS) spheres were assigned automatically so that the overlapping potentials would be the best possible approximations to the full potentials, and no interstitial sphere was necessary with the default 16% overlap restriction.[29] The WS radii determined by this procedure were reasonable: for $BaIrIn_4$, 2.34 Å for Ba; 1.55 Å for Ir; 1.79 Å and 1.80 Å for In1 and In2; and 1.50 Å for In3; and for $Ba_2Ir_4In_{13}$, 2.11 Å and 2.27 Å for Ba1 and Ba2; 1.53 Å for both Ir1 and Ir3; 1.52 Å and 1.54 Å for Ir2 and Ir4; 1.75 Å for In1; 1.49 Å for both In2 and In3; 1.65 Å for In4; 1.56 Å for In5; 1.62 Å for both In6 and In13; 1.71 Å for In7; 1.65 Å for In8; 1.51 Å for In9, In11, and In13; and 1.77 Å for In10.

(28) Tank, R.; Jepsen, O.; Burkhardt, A.; Andersen, O. K. *TB-LMTO-ASA Program*, version 4.7; Max-Plank-Institut für Festkörperforschung: Stuttgart, Germany 1995.

(29) Jepsen, O.; Andersen, O. K. *Z. Phys. B* **1995**, *97*, 35.

Results and Discussion

Crystal Structures. The structure of $BaIrIn_4$, Figure 1a, consists of a complex $_\infty^3[IrIn_4]^{2-}$ polyanion that encapsulates Ba cations within augmented pentagonal prisms constructed of In and Ir. The basic building unit, $Ba@IrIn_{12}$, Figure 1b, is a cation-centered pentagonal prism of indium on which two neighboring and the opposed rectangular faces are capped by In, In and Ir, respectively. The three capping atoms are coplanar with Ba and constitute the only so-called augmentation of the pentagonal prism. The relatively large cation proportion in this phase does not allow full-fledged augmentation, as in $SrRh_2In_8$.[22] Instead, condensation of the pentagonal prisms into zigzag chains occurs via sharing of their uncapped rectangular faces, Figure 1c. In addition, this structure can also be described[16] in other terms, namely, zigzag chains of *bcc*-like indium cubes $In3@In_8$ bicapped by Ir4 and condensed by face-sharing with iridium-centered trigonal prisms $Ir@In_6$ that are face-capped by the same In3, Figure 1c. The latter affords very short Ir−In3 distances (~2.60 Å, below). The cubes and trigonal prisms form zigzag chains separated by Ba layers, Figure 1c. This kind of description was used previously for $CaRhIn_4$, $CaIrIn_4$,[16] and $SrIrIn_4$[22] to emphasize the clear segregation of In therein and to show the structural relationship between $LaCoAl_4$-type phases and the binary compound $RhIn_3$.[30] Increases in cation sizes in the series $AeIrIn_4$, Ae = Ca, Sr, Ba, are primarily accommodated by increased puckering of the two intergrown chain types, c increasing in steps of 0.20 and 0.25 Å as a stays virtually constant and b increases somewhat less than changes in cation radii.

In contrast, the structure of $Ba_2Ir_4In_{13}$ ($Cmc2_1$) is made up of a more complex polyanion $_\infty^3[Ir_4In_{13}]^{4-}$ with Ba atoms encapsulated in two types of augmented prismatic cavities. The [100] view, Figure 2a, illustrates the general three-dimensional Ir−In network projected somewhat off the a axis. The structure can be described in terms of two basic building units: 20-vertex $Ba1@Ir_5In_{15}$ (blue) and 22-vertex $Ba2@Ir_7In_{15}$ (gray) polyhedra, Figure 2b,c, again with all atoms on mirror planes. However, these polyhedral descriptions are correct only in a formal, geometric sense. As can be seen in the [100] projection in Figure 2d, the radial distances from Ba to waist-capping Ir atoms are generally large, and some nonconvex angles arise as well. Otherwise, only face-capping In atoms are left about the prisms, and Ir is strongly bound only within the prism around Ba2 or in intervening trigonal prismatic In chains.

In a formal sense, the first polyhedron, Figure 2b, can be described as a pentagonal indium prism augmented by 10 regularly alternating Ir and In atoms in a decagon about the waist that are coplanar with Ba1, that is, a 5−10−5 arrangement of parallel planar rings. These stack along the a axis through shared basal faces. In the bc plane, Figure 2d, the 10-membered outer ring is seen to share two almost linear Ir3−In3−Ir1 edges with two other like rings to generate slightly zigzag chains of augmented pentagonal

(30) Pöttgen, R.; Hoffmann, R.-D.; Kotzyba, G. *Z. Anorg. Allg. Chem.* **1998**, *624*, 244.

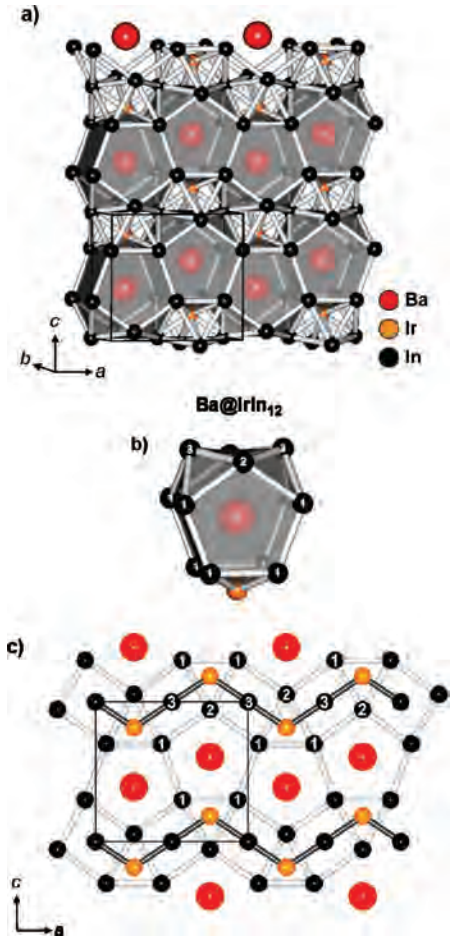

Figure 1. (a) General view of three-dimensional Ir−In network in orthorhombic BaIrIn$_4$ (*Pmma*). (b) The single basic building unit of the centered 13-vertex polyhedron, Ba@IrIn$_{12}$. (c) [010] view of the BaIrIn$_4$ structure in which the atoms interconnected by gray and white bonds lie in layers at $y = 0$ and $y = 1/2$, respectively. The connections between layers are not represented, for clarity.

prisms along the *c* axis, hereafter motif 1 (Figure 2a, blue section). Somewhat similar Sr@Rh$_5$In$_{15}$ building blocks have recently been reported in SrRh$_2$In$_8$,[22] which crystallizes in the CaCo$_2$Al$_8$ structure type.[31]

The second basic polyhedron, Ba@Ir$_7$In$_{15}$, Figure 2c, is a distorted Ba2-centered hexagonal prism made up of irregularly alternating Ir and In atoms, namely, Ir2, In12, Ir4, In14, In10, and In13. This too is augmented by a 10-membered ring, coplanar with Ba2, of seven In and three Ir atoms ordered as In11, In6, In7, In9, In13, Ir2, In2, Ir1, In5, and Ir4. The 6−10−6 arrangement of parallel planar rings, in this second unit, is novel. The Ba@Ir$_7$In$_{15}$ units also stack along the *a* axis by sharing basal faces. However, as seen in Figure 2d, each 10-membered outer ring of the Ba2@Ir$_7$In$_{15}$ unit now shares two opposite Ir−In edges with two six-membered rings of like neighbors that are displaced by *a*/2, as seen in perspective in Figure 2a. This leads to the formation of linear chains of noncoplanar hexagonal prisms along the *c* axis, motif 2 hereafter. Motifs 1 and 2 alternate along *b*, as shown in Figure 2a; the first are coplanar and identical, whereas the second alternate along *b* by *a*/2. This

(31) Czech, E.; Cordier, G.; Schaefer, H. *J. Less-Common Met.* **1983**, *95*, 205.

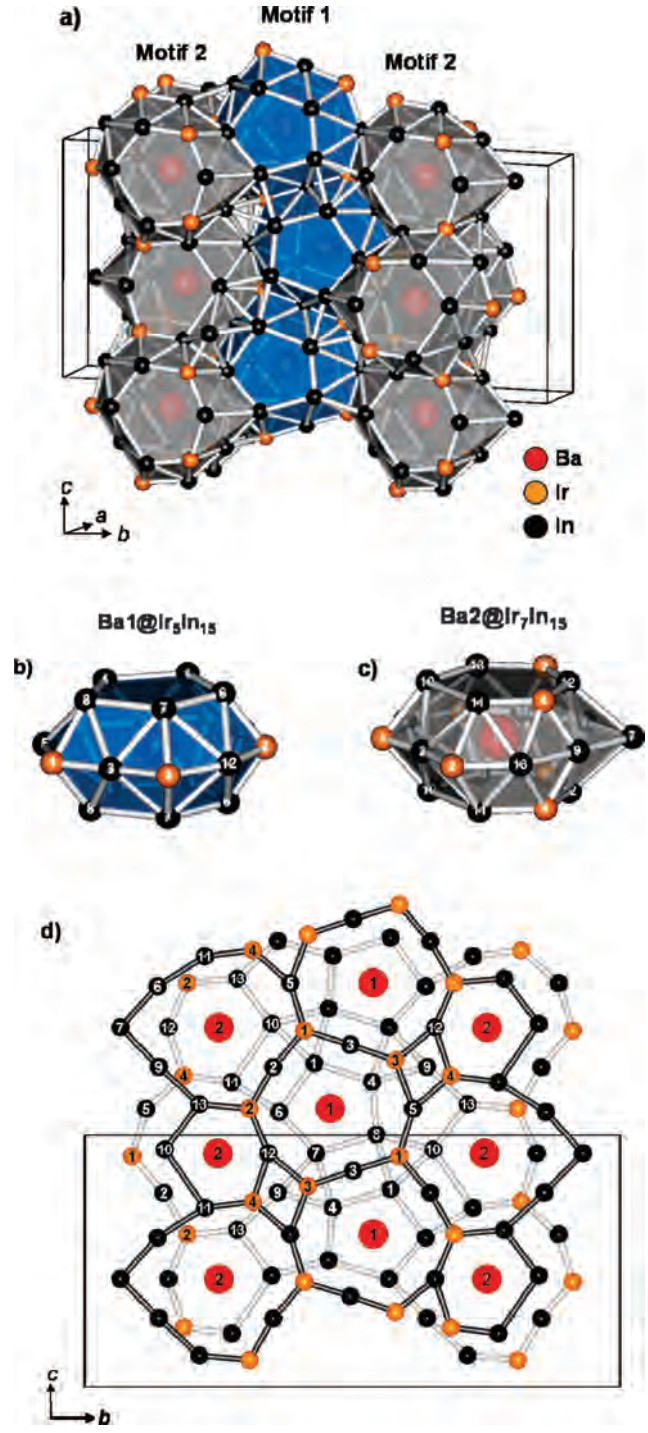

Figure 2. (a) General view of three-dimensional Ir−In network in Ba$_2$Ir$_4$In$_{13}$ (*Cmc*2$_1$). (b) The first formal building unit, the 20-vertex centered polyhedron, Ba@Ir$_5$In$_{15}$ (blue). (c) The second formal building unit, the 22-vertex centered polyhedron, Ba@Ir$_7$In$_{15}$. (d) [100] view of the crystal structure. The waist-capping Ir atoms are in fact weakly bonded to Ba. The atoms connected by black and gray lines lie at $y = 0$ and $y = 1/2$, respectively. The connections between layers are not shown for clarity.

becomes possible through rather complicated and irregular sharing of the edges of 10-membered rings of the first units. Besides two Ir3−In3−Ir1 edges which share identical polyhedra (see above), each 10-membered ring shares Ir1−In2 and In2−Ir2 edges with other (motif 1) 10-membered rings and Ir2−In12 edges with a six-membered ring of the second type of cluster, whereas the edge Ir1−In5

Table 3. Selected Bond Lengths [Å] and −ICOHP (eV/bond·mol) Values for $BaIrIn_4$ and $Ba_2Ir_4In_{13}$

$BaIrIn_4$			$Ba_2Ir_4In_{13}$					
bond	distance	−ICOHP	bond	distance	−ICOHP	bond	distance	−ICOHP
[a]Ir−In1	2.8500(6)	1.64	[a]Ir1−In1	2.916(2)	1.23	[a]In4−In5	3.513(3)	0.34
			Ir1−In2	2.625(3)	2.23	In4−In7	3.085(3)	0.67
[a]Ir−In2	2.8953(9)	1.37	Ir1−In3	2.610(3)	2.28	In4−In8	2.888(3)	1.73
			Ir1−In5	2.689(3)	2.16	In4−In9	3.093(3)	0.71
Ir−In3	2.6033(5)	2.42	[a]Ir1−In8	2.831(2)	1.55	[a]In5−In8	3.332(2)	0.59
			[a]Ir1−In10	2.904(2)	1.25	[a]In5−In9	3.280(3)	0.50
In1−In1	3.136(2)	0.76	Ir2−In2	2.599(3)	2.57	[a]In5−In10	3.326(3)	0.62
			[a]Ir2−In6	2.743(1)	1.90	[a]In5−In13	3.687(2)	0.20
In1−In1	3.390(2)	0.93	[a]Ir2−In11	2.848(2)	1.62	In6−In7	3.010(3)	1.39
			Ir2−In12	2.635(3)	2.47	In6−In11	3.035(3)	0.86
In1−In2	3.207(1)	0.55	Ir2−In13	2.733(2)	2.04	[a]In6−In12	3.218(2)	0.72
			Ir3−In3	2.604(3)	2.45	In7−In8	3.436(3)	0.35
In1−In2	3.363(1)	0.86	[a]Ir3−In4	2.841(2)	1.63	In7−In9	2.991(3)	0.87
			Ir3−In5	2.798(3)	1.78	[a]In7−In13	3.391(2)	0.44
In1−In3	3.2824(7)	0.53	[a]Ir3−In7	2.903(2)	1.41	In8−In10	3.181(3)	0.60
			[a]Ir3−In9	2.822(2)	1.43	[a]In9−In12	3.136(2)	0.66
[a]In2−In3	3.1121(5)	0.89	Ir3−In12	2.791(2)	1.64	In9−In13	2.989(3)	0.96
			Ir4−In5	2.703(3)	2.07	In10−In11	3.836(3)	0.31
[b]Ba−Ir	3.355(1)		[a]Ir4−In9	2.643(2)	2.07	In10−In13	3.099(3)	1.21
			Ir4−In11	2.637(2)	2.64	[a]In11−In13	3.079(2)	0.80
Ba−In1	3.5982(8)		Ir4−In12	2.773(3)	1.80	Ba1−In1	3.450(3)	
			[a]Ir4−In13	2.859(2)	1.62	[b]Ba1−In2	3.837(3)	
Ba−In1	3.6408(9)		Ir3−Ir4	3.102(2)	0.83	[b]Ba1−In3	3.596(4)	
			[a]In1−In2	3.142(2)	0.79	[b]Ba1−In3	3.636(4)	
Ba−In2	3.456(1)		[a]In1−In3	3.170(2)	0.72	Ba1−In4	3.491(2)	
			In1−In4	3.301(3)	0.91	Ba1−In6	3.606(2)	
[b]Ba−In3	3.7779(9)		In1−In6	3.257(4)	1.00	Ba1−In7	3.401(3)	
			In1−In8	3.075(3)	0.71	Ba1−In8	3.624(2)	
			In1−In10	3.152(3)	0.60	[b]Ba2−Ir2	3.745(2)	
			[a]In2−In6	3.326(2)	0.48	Ba2−Ir4	3.972(2)	
			[a]In2−In10	3.254(2)	0.63	[b]Ba2−In2	3.647(3)	
			[a]In2−In11	3.296(2)	0.58	[b]Ba2−In6	4.019(3)	
			[a]In3−In4	3.219(2)	0.60	[b]Ba2−In9	3.895(3)	
			[a]In3−In7	3.186(2)	0.68	Ba2−In10	3.619(2)	
			[a]In3−In8	3.223(2)	0.63	Ba2−In11	3.778(3)	
						[b]Ba2−In11	3.953(3)	
						Ba2−In12	3.583(2)	
						[b]Ba2−In13	3.618(2)	

[a] Bonds between basal and waist atoms. [b] Distances between Ba and waist atoms.

is shared with 10-membered ring of the motif 1 chain, Figure 2d.

The overall drive for the formation of such a complex structure can be interpreted as the need to give each Ae cation as many close T and In neighbors as possible in the more anionic network as well as to alternate Ir and In atoms so far as possible. This depends on the stoichiometry and the relative Ae sizes and contents as well as on the flexibility of an anionic network, and an optimal though complex condensation mode. The principle was evidently first put forth for the monoclinic structure of $SrIn_4$,[32] and parallel interpretations have been given to orthorhombic $BaAu_2Tl_7$,[10] $(Ba,Sr)Au_2In_2$,[13] and others. With greater Ae contents, as in $BaIrIn_4$, the waist augmentation of pentagonal prisms often cannot reach 10 or more atoms, and this leads to direct contact between five-member rings. On the other hand, with the lower Ae proportions in $Ba_2Ir_4In_{13}$ or $SrRh_2In_8$,[22] the five-membered rings are separate because there is enough indium to complete the augmentation of pentagonal prisms. However, in $Ba_2Ir_4In_{13}$, the whole structure cannot be built from "ideal" 5−10−5 polyhedra, as in $CaCo_2In_8$-type compounds. The relatively large size of Ba as well as greater Ir content lead to the creation of augmented hexagonal $Ba@Ir_7In_{15}$ polyhedra, which is new for Ae−T−In phases. It is important to notice that in $Ba_2Ir_4In_{13}$ there is also a clear segregation of the indium atoms into distorted centered In3@In8 *bcc* cubes within motif 1 and centered $In5@In_{10}$ pentagonal prisms situated between the two motifs. Pentagonal prismatic indium coordination in alkaline-earth metal phases has been observed before only in a few cases, $CaCo_2In_8$-type indides $SrRh_2In_8$[22] and $EuRh_2In_8$.[33]

In both structures, the heteroatomic Ir−In bond distances are similar, 2.60−2.90 Å in $BaIrIn_4$ and 2.60−2.92 Å in $Ba_2Ir_4In_{13}$, Table 3, comparable to those in $CaIrIn_4$ (2.61−2.87 Å),[16] $SrIrIn_4$ (2.61−2.88 Å),[22] $CaIrIn_2$ (2.71−2.80),[34] $SrIrIn_2$ (2.71−2.81),[35] and $BaIrIn_2$ (2.80 Å).[36] The short and evidently strong Ir−In interactions (below) also reflect their disparate Mulliken electronegativities:[37]for Ae = Ca, Sr, and Ba, 2.2, 2.00, and 2.4; for In, 3.1; and for Ir, 5.8 eV. These are obviously very important factors in the formation of numerous compounds of this nature. The present single

(32) Seo, D.-K.; Corbett, J. D. *J. Am. Chem. Soc.* **2000**, *122*, 9621.
(33) Pöttgen, R.; Kussmann, D. *Z. Anorg. Allg. Chem.* **2001**, *627*, 55.
(34) Hoffmann, R.-D.; Pöttgen, R. *Z. Anorg. Allg. Chem.* **2000**, *626*, 28.
(35) Hoffmann, R.-D.; Rodewald, U. Ch.; Pöttgen, R. *Z. Naturforsch. B* **1999**, *54*, 38.
(36) Hoffmann, R.-D.; Pöttgen, R. *Chem.—Eur. J.* **2001**, *7*, 382.
(37) Pearson, R. G. *Inorg. Chem.* **1988**, *27*, 736.

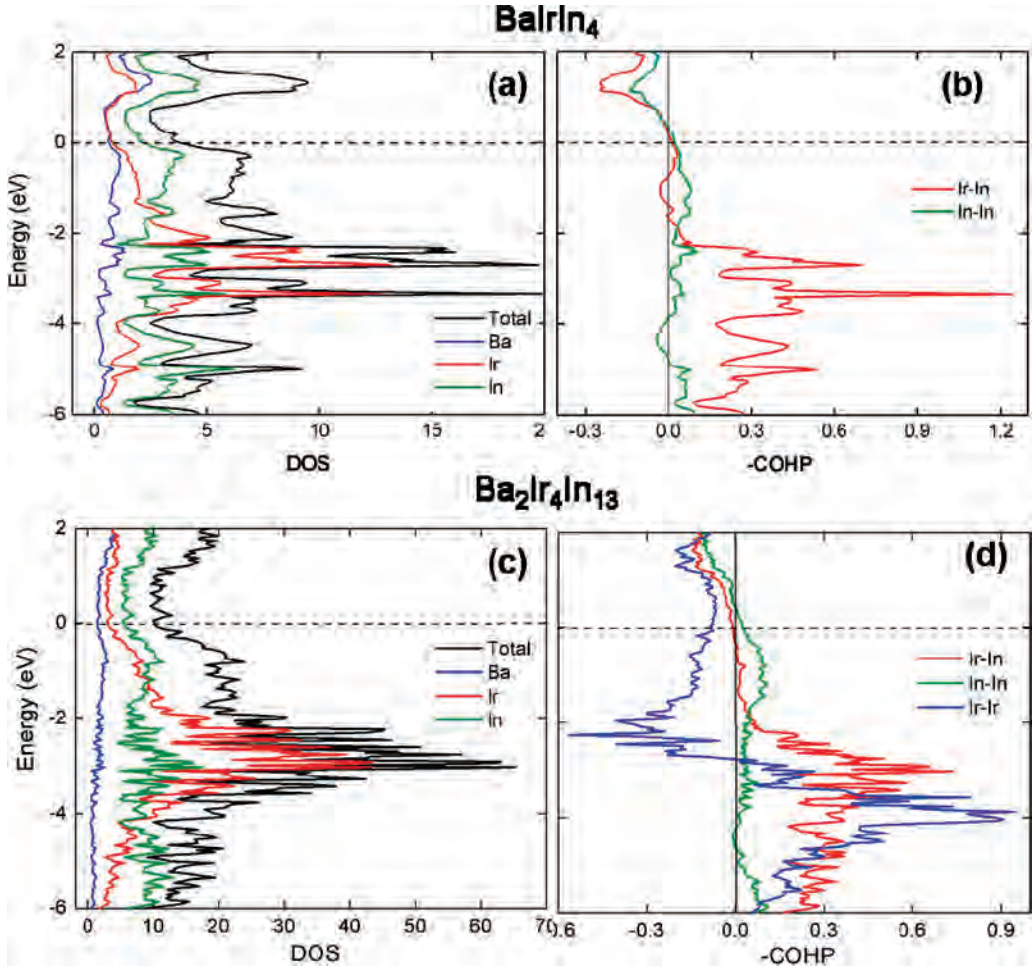

Figure 3. TB-LMTO-ASA electronic structure calculation results for BaIrIn$_4$ and Ba$_2$Ir$_4$In$_{13}$. The dashed lines denote the Fermi levels. (a, c) Total DOS (black) and partial DOS curves for Ba (blue), Ir (red), and In (green). (b, d) −COHP data for each of three different interactions, per bond·mole: Ir−In (red), In−In (green), Ir−Ir (blue). The numbers of contacts of each type per cell are 10, 8, and 0 in BaIrIn$_4$ and 32, 48, and 1 in Ba$_2$Ir$_4$In$_{13}$.

example of an Ir−Ir contact, that is, Ir3−Ir4 (3.102(2) Å) in Ba$_2$Ir$_4$In$_{13}$, occurs across Ir$_2$In$_2$ parallelograms between every pair of coplanar 10-membered and six-membered rings, Figure 2d. This secondary contact is a weak bonding interaction, much longer than the Pauling single bond length, 2.53 Å,[38] and is presumably determined by packing restraints (below). Finally, both compounds have several types of In−In contacts, including those within the basal five-membered or six-membered rings, planar separations between those rings, and prism−waist contacts, Table 2 and Figures 1c, 2d. The In−In distances of BaIrIn$_4$ are in the range of 3.11−3.39 Å, which is typical for other Ae−Ir−In-network compounds[16,22,34−36] with In−In distances usually in the range of 3.1−3.4 Å. The unusual small In4−In8 distance of 2.888(3) Å in Ba$_2$Ir$_4$In$_{13}$ is also reflected in a large bond population (below). Very complex bonding and packing interactions are represented in these structures.

Electronic Structure and Chemical Bonding. The densities-of-states (DOS) for both of the title compounds, Figure 3a,c, exhibit broad bands with low but finite DOS values around E$_F$, indicating metallic characteristics. The iridium d bands remain fairly narrow in both BaIrIn$_4$ and Ba$_2$Ir$_4$In$_{13}$ phases and are centered near −3 eV, mixing with very broadened In states. In contrast, the Au d bands in diverse A/Ae−Au−In phases are distinctly broader and fall at lower energies.[13,39−41]

Crystal orbital Hamilton populations (−COHP) were evaluated, as shown in Figure 3b and d for BaIrIn$_4$ and Ba$_2$Ir$_4$In$_{13}$, respectively, to describe the interactions between atom pair types. Note that each is plotted per contact, not for the sum. In BaIrIn$_4$, both Ir−In and In−In bonding interactions are practically optimized at the Fermi level, although a few empty bonding In−In and Ir−In states nearby might allow some electron addition, and so the existence of isostructural BaPtIn$_4$ could be assumed. However, this simple assessment neglects all important considerations regarding the stability of alternate phases, and in fact, the suggested phase occurs in the alternate LaCoAl$_4$ structure type found with electron-richer analogs (see the Introduction).[43] In Ba$_2$Ir$_4$In$_{13}$, strong In−In bonding remains at E$_F$, whereas both Ir−Ir and Ir−In bonding is almost optimized, Figure 3d. Adding more electrons to Ba$_2$Ir$_4$In$_{13}$ (by substitution of Ir

(38) Pauling, L. *Nature of the Chemical Bond*, 3rd ed.; Cornell University Press: Ithaca, NY, 1960; p 403.
(39) Li, B.; Corbett, J. D. *Inorg. Chem.* **2007**, *46*, 6022.
(40) Lin, Q.; Corbett, J. D. *J. Am. Chem. Soc.* **2007**, *129*, 6789.
(41) Lin, Q.; Corbett, J. D. *Inorg. Chem.* **2007**, *46*, 8722.
(42) Palasyuk, A.; Dai, J.-C.; Corbett, J. D. *Inorg. Chem.* **2008**, *47*, 3128.
(43) Palasyuk, A.; Corbett, J. D. Unpublished research.

by Pt, for example) might be possible through the filling of bonding In−In states, though these are likely the weakest of the group (Table 3).

The integrated crystal overlap Hamilton populations (−ICOHP) were also determined for all pairwise interactions, Table 3. All of the −ICOHP values are reasonable and more or less inversely parallel to their bond distances for each bond type. Those for Ir−In in both compounds are quite large, more than 1.3 eV/bond·mol, suggesting their dominance in structural stabilization. The −ICOHP values for In−In bonds in both structures fall in the range of 0.5−1.0 eV/bond·mol, which is typical and comparable to those in other Ae−T−In indides.[42] In $Ba_2Ir_4In_{13}$, though, there are some extremes: the significantly short In4−In8 distance of 2.89 Å in basal indium pentagons corresponds to 1.73 eV/bond·mol, whereas contacts In4−In5, In5−In13, and In10−In11 at 3.51, 3.69, and 3.84 Å cannot be assessed as nonbonding because of small, though positive −ICOHP values of 0.34, 0.20, and 0.31 eV/bond·mol, respectively. That for the only Ir−Ir distance of 3.10 Å is fairly large, 0.83 eV/bond·mol.

Acknowledgment. This research was supported by the Office of the Basic Energy Sciences, Materials Sciences Division, U.S. Department of Energy (DOE). The Ames Laboratory is operated for DOE by Iowa State University under Contract No. DE-AC02-07Ch11358.

Supporting Information Available: Comparison of observed and calculated powder patterns for $BaIrIn_4$ and $Ba_2Ir_4In_{13}$ and their crystallographic refinement parameters in CIF format. This material is available free of charge via the Internet at http://pubs.acs.org.

IC8006124